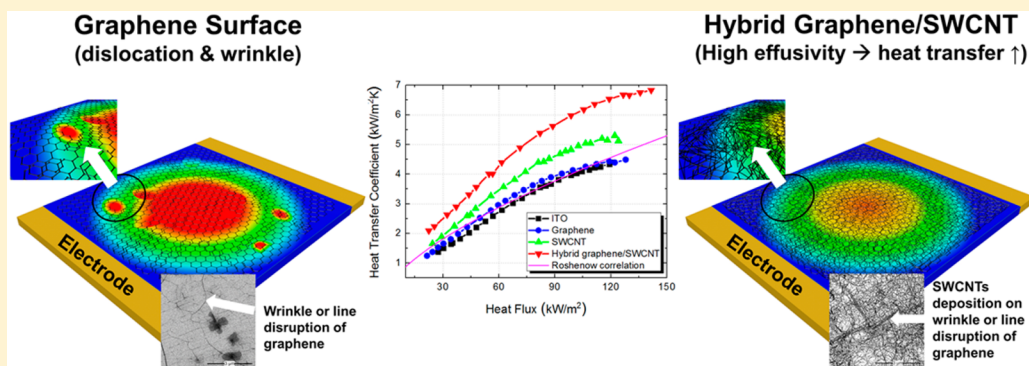


Hybrid Graphene and Single-Walled Carbon Nanotube Films for Enhanced Phase-Change Heat Transfer

Han Seo,[†] Hyung Duk Yun,[‡] Soon-Yong Kwon,[‡] and In Cheol Bang^{*,†}

[†]School of Mechanical and Nuclear Engineering and [‡]School of Materials Science and Engineering, Ulsan National Institute of Science and Technology (UNIST), Ulsan 689-798, Republic of Korea



ABSTRACT: Nucleate boiling is an effective heat transfer method in power generation systems and cooling devices. In this letter, hybrid graphene/single-walled carbon nanotube (SWCNT), graphene, and SWCNT films deposited on indium tin oxide (ITO) surfaces were fabricated to investigate the enhancement of nucleate boiling phenomena described by the critical heat flux and heat transfer coefficient. The graphene films were grown on Cu foils and transferred to ITO surfaces. Furthermore, SWCNTs were deposited on the graphene layer to fabricate hybrid graphene/SWCNT films. We determined that the hybrid graphene/SWCNT film deposited on an ITO surface is the most effective heat transfer surface in pool boiling because of the interconnected network of carbon structures.

KEYWORDS: Graphene, SWCNTs, hybrid graphene/SWCNTs, boiling heat transfer, critical heat flux

Graphene, which has a single layer of carbon atoms with an sp^2 hybrid structure, has superior electrical, mechanical, and thermal properties compared with transparent heaters such as indium tin oxide (ITO).^{1–5} Chemical vapor deposition (CVD) has been extensively studied as a graphene layer formation method for use in the synthesis of graphene. In the CVD method, graphene films were formed on Cu foil and showed more effective heat removal than conventional transparent ITO heaters in heating and cooling procedures in the air.⁶ In recent times, the combination of graphene and carbon nanotubes (CNTs) has been widely studied because such combined surface can enhance the conductivity by incorporating carbon structures.^{7–11} By connecting graphene and CNTs, the sheet resistance of the surface of the combined materials is lower than that of the graphene-only surface. Additionally, a different method of growing physically deposited graphene layers on a substrate has been studied using a rapid thermal annealing (RTA) method.¹² The graphene grown with the RTA method was composed of a few layers and was not uniformly distributed over large areas. The surface morphology of the graphene appeared as patches of different thicknesses, revealing that the graphene films formed as a result of the surface segregation of excess carbon at the nickel surface after the vacuum RTA process.¹³ Graphene films on substrates have been studied in terms of the

enhancement of electrical and thermal performance under atmospheric conditions.

In the boiling experiment using graphene layers, different deposition methods were used. Instead of the CVD and RTA methods, graphene layer deposition on heating surfaces, graphene, graphene oxide, and reduced graphene oxide nanofluids was studied in a boiling experiment to enhance the CHF and BHT. Graphene oxide and graphene nanofluids were used to enhance the thermal limit by comparing the base fluid with other nanofluids.¹⁴ The deposition of the graphene oxide and graphene nanoparticles on the heating surface during the boiling process could enhance the CHF because of the change in the modulation wavelength and the thermal properties of the heating surfaces with highly thermally conductive porous structures.¹⁴ The thickness effects of graphene layers were studied to show the influence of the thickness of graphene films during the boiling process.^{15,16} The thickness of the graphene films was controlled by the amount of reduced graphene oxide colloid, and the graphene-coated film heaters enhanced the CHF and BHT. The thermal activity

Received: September 21, 2015

Revised: December 27, 2015

and thermal diffusivity parameters were considered to be factors enhancing the CHF and activating nucleation sites.^{15,16} Recently, two types of graphene surfaces were applied to the pool boiling experiment: few-layer graphene with an RTA fabrication method and the deposition of graphene nanoparticles on the heating surfaces.¹³ The results indicated that the porous graphene-coated (nanoparticle-coated) surface showed improvement in the CHF and BHT, whereas the nonporous graphene surface (RTA method) did not show enhanced CHF and BHT.¹³ The presence of graphene patches with different layers in the nonporous few-layer graphene on the heating surface could suppress the highly conductive property of the graphene. To compensate for the dislocation of the graphene surface, a hybrid surface was fabricated by coating a nonporous graphene surface with single-walled carbon nanotubes (SWCNTs). Instead of the RTA method, the CVD method was used to grow the graphene layers because CVD-fabricated graphene layers develop uniformly on a substrate. Previous studies related to the combining graphene/CNTs surface have been indicated that the hybrid surface shows a synergistic conduction effect of combining one-dimensional CNT and two-dimensional graphene.^{7–11} Here, we report on the first ever study of the pool boiling of a hybrid graphene/SWCNT layer, deposited on an ITO surface, and observed significant enhancement of the heat transfer coefficient (HTC) compared with other heating surfaces used in the experiment. As a measurement system for the boiling performance, infrared (IR) thermography was used.

Four types of heating surfaces were prepared and examined in the pool boiling facility: (1) a bare ITO surface, (2) graphene, (3) SWCNT, and (4) hybrid graphene/SWCNT layers on ITO surfaces. ITO layer is opaque in the IR range (3–5 μm), and thus, the investigation of heating surface temperature fields using IR thermometry is possible. Sapphire (50 mm \times 50 mm) was used as the substrate material because it has high optical and thermal transmission.^{13,17} On the sapphire substrate, an ITO layer with a thickness of 750 nm was deposited by vacuum deposition with an area of 50 mm \times 32 mm. Silver electrodes (9 mm \times 32 mm) were deposited at the end of the ITO layer. Therefore, the heating area of the bare ITO surface was 32 mm \times 32 mm. Three types of heater surfaces were fabricated on the bare ITO surfaces. For the graphene films deposited on the bare ITO surface, we used Cu foil with a thickness of 25 μm and an area of 40 mm \times 40 mm to grow the graphene films. Figure 1a shows the fabrication process of the graphene growth. Cu foil was placed in a CVD chamber and heated with a flow of H₂ to enlarge the Cu grains. After annealing, a gas mixture of CH₄ and H₂ was introduced into the chamber. Finally, the sample was cooled from the growth temperature to 500 °C and then rapidly cooled to room temperature. A poly(methyl methacrylate) (PMMA) solution was spin coated on the as-grown graphene films on the Cu foil to etch the graphene film from the Cu foil. The remaining PMMA/graphene was washed with fresh distilled water, placed on the target substrate (ITO surface), and dried. After transferring it to the target substrate, acetone was applied to remove the PMMA. For the hybrid graphene/SWCNT layers, a simple spray coating of SWCNTs was used on a graphene surface. Figure 1b illustrates the SWCNT coating method on the bare ITO and graphene surfaces. Arc-made SWCNTs dispersed in distilled water were purchased from Nanosolution, Korea, with diameters and lengths of 1.4–1.7 nm and 5–20 μm , respectively. Prior to SWCNT solution coating, the target

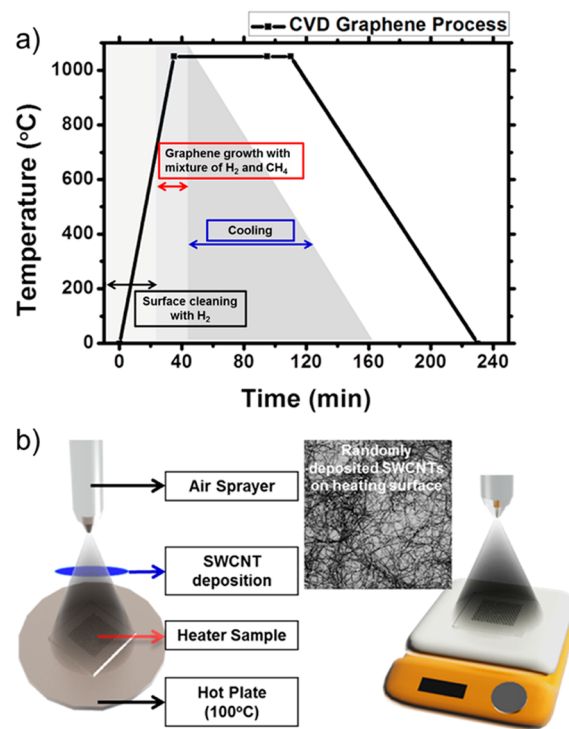


Figure 1. Hybrid graphene/SWCNT layer fabrication: (a) graphene growth process and (b) SWCNTs coating on a substrate.

substrate was first rinsed in an acetone and isopropyl alcohol (IPA) bath for 5 min in an ultrasonicator, and the solvents were then gently blown away. To spray the SWCNTs in a uniform coat, the substrate was placed on a hot plate at 100 °C and sprayed using an air brush with a nozzle of 0.3 mm in diameter. The SWCNT-coated substrate was then dipped in distilled water for 30 min to remove the surfactant, and then gently blown with a N₂ gun. The SWCNT quantity was set to 4 μL because we confirmed that the optimized and saturated sheet resistance of the hybrid films was achieved when this quantity was used for the coat. To compare the hybrid graphene/SWCNT layers, only SWCNTs were sprayed on the ITO surface to decouple the effects of the interconnection of the graphene and SWCNTs. The same SWCNT quantity was deposited on an ITO surface.

Figure 2 compares scanning electron microscopy (SEM) images of the ITO, graphene, SWCNT, and hybrid graphene/SWCNT surfaces. Figure 2a shows the ITO surface, which had a nanosmooth surface without having microcavities. Figure 2b shows the graphene surface that was transferred to the ITO surface. The difference in brightness levels indicates the graphene density, and the lines in the image could be considered as wrinkles or disconnected areas in the graphene. Figure 2c shows the SWCNTs deposited on the bare ITO surface, demonstrating that they were randomly positioned. The surface of the hybrid graphene/SWCNT heater is shown in Figure 2d. SWCNTs were randomly deposited on the graphene surface and connected where the wrinkles or disconnected lines were located on the graphene surface. Surface roughness was characterized using atomic force microscopy (AFM) because the roughness affects the boiling performance. Figure 3 shows the AFM images and the illustrations of all heating surfaces. The arithmetic average of the surface height deviation (R_a) and the root-mean-square roughness (R_q) were used as the surface roughness parameters

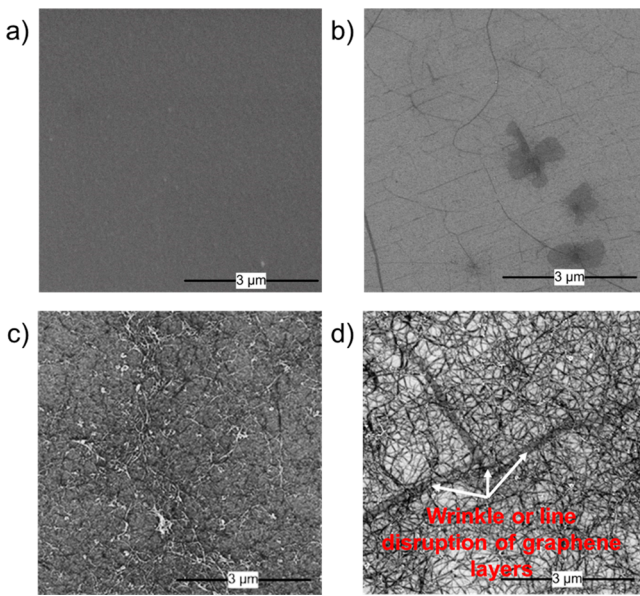


Figure 2. SEM images of (a) ITO, (b) graphene, (c) SWCNTs, and (d) hybrid graphene/SWCNT surfaces.

($10 \mu\text{m} \times 10 \mu\text{m}$). The values of R_a and R_q for the bare ITO heater (Figure 3a) were 9.4 and 12.1 nm, respectively, and those for the graphene heater (Figure 3b) were 11.2 and 14.5 nm, respectively. Additionally, the values of R_a and R_q for the SWCNTs heater (Figure 3c) were 10.9 and 14.0 nm, respectively, and those for the hybrid graphene/SWCNT heater (Figure 3d) were 5.04 and 7.61 nm, respectively. Side views of all heating surfaces are illustrated in the AFM images below (Figure 3). By overlapping the graphene and SWCNTs on the bare ITO surface, the roughness of the hybrid graphene/SWCNT surface may be decreased. There was no obvious difference in surface roughness for the graphene, SWCNTs, and hybrid graphene/SWCNTs heating surfaces compared with the

bare ITO surface. This demonstrates that the surface roughness of the ITO surfaces did not change after the deposition of the graphene and SWCNT layers.

The experiment was conducted in atmospheric pressure using the refrigerant FC-72. Four cartridge heaters were in the boiling vessel to maintain the saturation state of the working fluid through proportional integral differential (PID) control. During the experiment, the temperature of the working fluid was continuously monitored by thermocouples to maintain the FC-72 at its saturation point. To measure the temperature fields of the various heating surfaces, IR thermometry was used. The IR intensity from the heating surfaces was delivered to the IR thermometry via a gold-coated reflection mirror. To obtain the exact temperature fields of the heater surface, we matched the IR intensity to the temperatures of the heater surfaces used for the bare ITO, graphene, SWCNTs, and hybrid graphene/SWCNT layers, which were measured by a K-type thermocouple. The maximum error of temperature measurement was less than 0.5 °C. The temperature distributions of the heater surfaces, boiling curve, HTC, and CHF phenomena were observed in the experiment. To supply power to the heating surfaces, a DC power supply with a capacity of 5.25 kW (150 V, 35 A) was connected to the heater electrodes through copper blocks. The power supplied to the heating surfaces was increased stepwise until the CHF point was reached. The current passing through the heating surface was measured by a standard resistor. The voltage and current data were read by the data acquisition system, and the heat flux of the heating surfaces was calculated. During the experiment, the sheet resistance of the graphene, SWCNTs, and hybrid graphene/SWCNT heating surfaces was similar to the bare ITO surface. This means that the interface resistance of the deposition layer was not observed when the heat or power was applied on the heating surfaces. The major parameters of the CHF and BHT were obtained using IR thermometry.

The CHF phenomenon in the plate pool boiling facility always appeared with a sudden increase in the temperature of

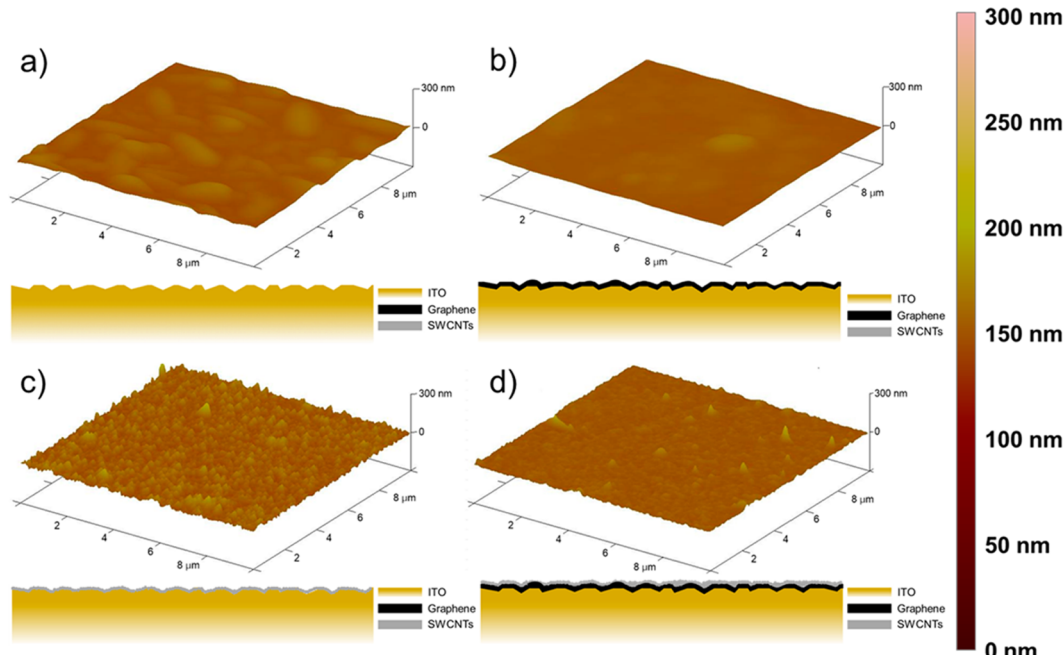


Figure 3. AFM images and side views of (a) ITO, (b) graphene, (c) SWCNTs, and (d) hybrid graphene/SWCNT surfaces.

the heater surface. As the CHF was approached, bubble coalescence occurred and vapor films formed on the heater surface. Because the vapor has a lower heat transfer ability than the liquid, the temperature of the heating surface increased rapidly at the CHF point. Therefore, the CHF point was defined as the point where the heating surface temperature increased dramatically. This phenomenon is also called the phase-change limit. Figure 4a depicts the boiling curves of the

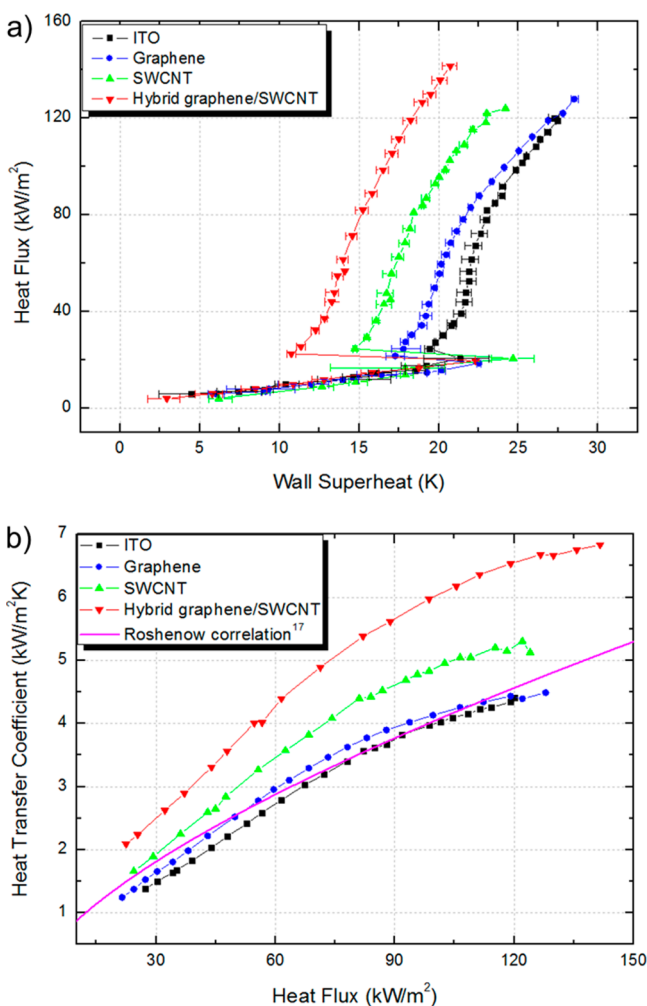


Figure 4. (a) Boiling curves for ITO, graphene, SWCNTs, and hybrid graphene/SWCNT heating surfaces. (b) Heat transfer coefficients for ITO, graphene, SWCNTs, and hybrid graphene/SWCNT heating surfaces.

bare ITO, graphene, SWCNTs, and hybrid graphene/SWCNT heaters. The boiling curve of the bare ITO heater was provided as a basis of comparison for the boiling performance. The error bars indicated in the boiling curves represent the ranges of the wall superheat at each heat flux using various samples. The CHF phenomenon can be introduced by many theories including hydrodynamic instability, macrolayer dryout, hot and dry spots, and bubble interaction. Hydrodynamic instability model has been widely used in the CHF prediction model, which attributes the phenomenon of the critical vapor velocity to the phase-change limit.¹⁸ As the applied heat rises, the velocity vapor departure from the heating surface increases. The departure of the vapor causes a resistance between the vapor and the liquid interface. When the velocity of the vapor

exceeds the critical value, the liquid could not be supplied to the heating surface, and CHF occurs. Therefore, Zuber proposed the hydrodynamic instability model based on the critical value of the vapor velocity.¹⁸

$$q''_{CHF} = \frac{\pi}{24} \rho_g^{1/2} h_{lg}^{1/4} g \sigma (\rho_l - \rho_g) \quad (1)$$

where ρ_l and ρ_g are the liquid and vapor densities, respectively, h_{lg} is the latent heat of the working fluid, and σ is the surface tension of the working fluid. The predicted CHF with FC-72 on a two-dimensional surface was calculated as 148.15 kW/m^2 based on the hydrodynamic instability model. The CHF value of the bare ITO surface was obtained 119.8 kW/m^2 , which value was similar to the prediction model. By comparing the CHF values of the bare ITO heater to the prediction model, the experiment proved the reliability because the bare ITO heater was used as a basis of comparison for other heating surfaces.

In the experimental results, the CHF values of the graphene, SWCNTs, and hybrid graphene/SWCNT heaters were found to be 130.5 , 123.0 , and 141.6 kW/m^2 , respectively. Of the investigated heaters, the hybrid graphene/SWCNT heater achieved the maximum enhancement of the CHF in comparison with the bare ITO heater (18.2%). Conversely, the phase-change limit of the graphene and SWCNTs heaters was similar to that of the bare ITO heater. The CHF results of the graphene surface were similar to those for the graphene surface developed by the RTA method.¹³ This means that the thickness of the graphene layer within the nanometer had no impact on the CHF and BHT performance. That is, the superior thermal properties of the graphene were not exhibited because disconnected lines and wrinkles were present, as shown in Figure 2b. In addition, the main factor causing the difference between the CHF performances of the nanoparticle-coated surface and the physically deposited graphene layer was the coating thickness. The enhancement of the CHF in previous graphene nanofluids experiments was attributed to surface modifications such as the deposition of particles on heating surfaces with microscale thicknesses and porous structures.^{13–16} In the present work, however, the coating thickness of the graphene, SWCNTs, and hybrid graphene/SWCNTs was in the nanoscale range with nonporous structures. This means that the coating thickness and the porous structures are the major parameters influencing the CHF performance.

However, with regard to heat transfer performance at a similar heat flux, significant improvement to the HTC was observed in the hybrid graphene/SWCNT heater. Figure 4b shows the BHT performance based on the HTC. For the nucleate boiling performance, Rohsenow¹⁹ proposed the following equation:

$$\frac{C_{pl}\Delta T}{h_{lg}} = C_{sf} \left\{ \frac{q''}{h_{lg}\mu_l} \left[\frac{\sigma}{g(\rho_l - \rho_g)} \right]^{1/2} \right\}^m \left(\frac{C_{pl}\mu_l}{k_l} \right)^n \quad (2)$$

where C_{pl} is the liquid specific heat, h_{lg} is the latent heat, C_{sf} is the surface fluid combination, μ_l is the dynamic viscosity, k_l is the liquid conductivity, and m and n are the exponents of the Rohsenow correlation. The correlation was compared with the bare ITO because the coated surfaces could change the surface fluid combination. The Rohsenow correlation showed that the experiment with the ITO surface showed a similar trend. As shown in Figure 4b, more effective heat transfer was demonstrated on the hybrid graphene/SWCNT heater surface

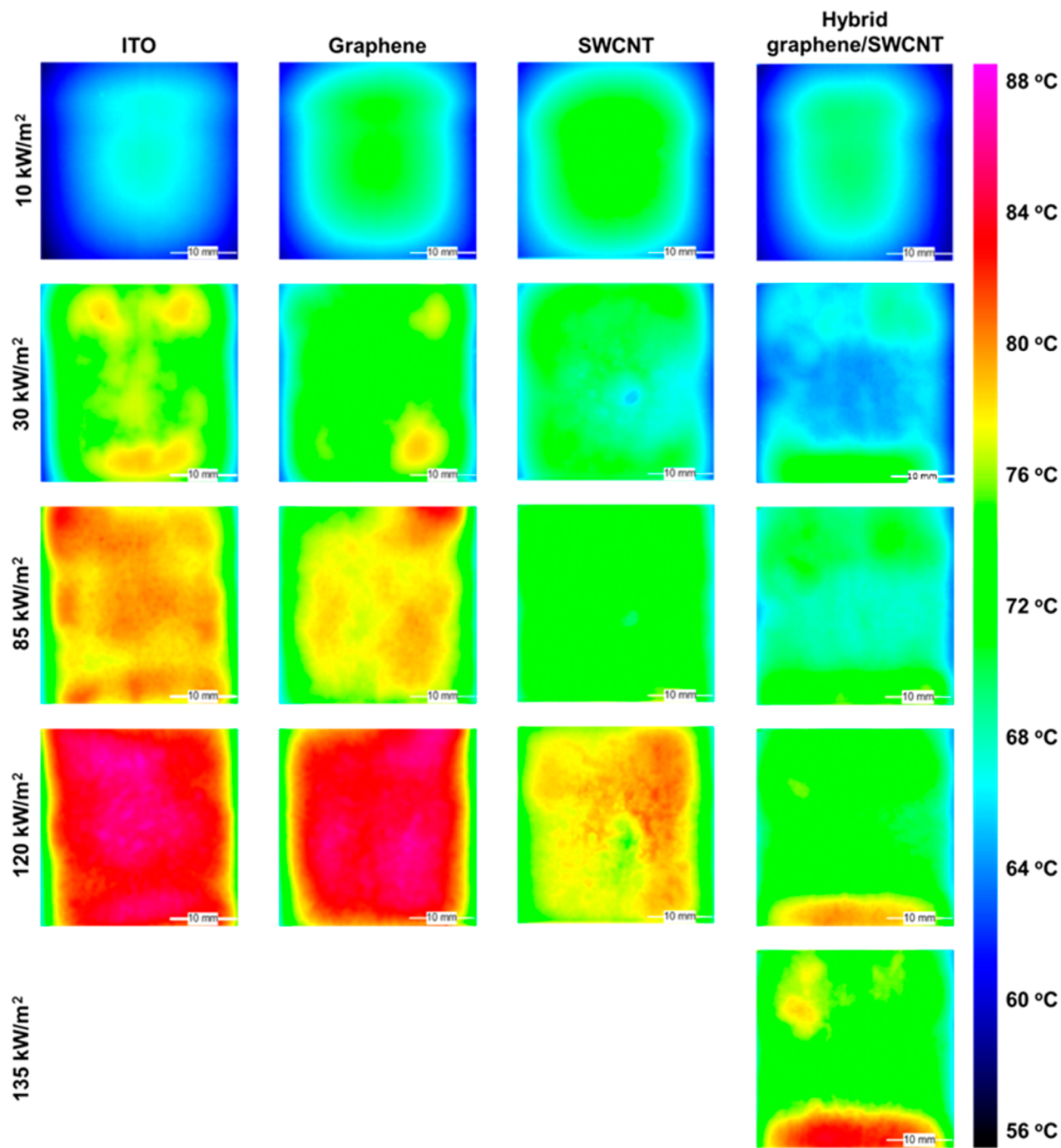


Figure 5. Temperature distribution on heater surfaces at various heat fluxes for ITO, graphene, SWCNTs, and hybrid graphene/SWCNT surfaces.

compared with other heater surfaces. Figure 5 shows the temperature distribution of the heating surfaces at various heat fluxes (10, 30, 85, 120, and 135 kW/m²). As Figure 5 indicates, the maximum and average temperatures of the hybrid graphene/SWCNT heater were lower than those of the other heating surfaces. For the SWCNTs heater, the BHT was also enhanced compared to the bare ITO and graphene heating surfaces. Conversely, the onset of the nucleate boiling region was similar for every heating surface: 24, 22, 24, and 23 kW/m² for the bare ITO, graphene, SWCNTs, and hybrid graphene/SWCNT heaters, respectively. The average wall superheat required for bubble departure was 10.7 °C for the hybrid graphene/SWCNT heater. The wall superheat of the

graphene/SWCNT heater was the lowest among the heater surfaces (19.4, 17.3, and 14.7 °C for the ITO, graphene, and SWCNT heaters, respectively). These results indicate that the effective heat dissipation on the heater surface and the heat conduction to the fluids appeared in the hybrid graphene/SWCNT heating surface.

The maximum HTC values of the bare ITO, graphene, SWCNTs, and hybrid graphene/SWCNT heaters were measured as 4.41, 4.49, 5.31, and 6.83 kW/m²K, respectively. As shown in Figure 4a, the boiling curve of the graphene surface was similar to that of the ITO surface. The graphene surface, which was deposited on the ITO surface with a thickness on the order of nanometers, did not affect the CHF

and BHT. Furthermore, graphene layers can have wrinkles and disconnected lines on the layers during the graphene growth process. These disconnected lines deteriorate the high-conduction performance of the graphene layer and do not result in the enhancement of the CHF and HTC. To compensate for the effects of the wrinkles and disconnected lines on the graphene surface, SWCNTs were deposited randomly on the graphene surface to connect the graphene dislocation areas and maximize thermal performance. Figure 2d shows the hybrid graphene/SWCNT heating surface. When the SWCNTs were randomly deposited on the graphene surface, they made connections where the wrinkles and disconnected lines were located. The thick black lines in Figure 2d are disruptions in the graphene films that deteriorated the thermal properties of the graphene. These disruptions were covered by the SWCNTs. By incorporating SWCNTs into the graphene, we decreased the sheet resistance and increased the electrical conductivity of the hybrid graphene/SWCNT surface, ultimately obtaining a highly conductive surface. The hybrid graphene/SWCNT surface maximized the heat dissipation performance. The boiling performance was also enhanced, as shown in the boiling curves. To decouple the effects of the hybrid graphene/SWCNT layers, the SWCNT heating surface was used to show the effects of the SWCNTs on the CHF and HTC. As shown in Figure 4a,b, an enhanced HTC was obtained, but the CHF did not show any improvement. The maximum HTC for the SWCNTs heater was higher than those of the graphene and ITO heaters, but lower than that of the hybrid graphene/SWCNT heater. When the SWCNTs were deposited on the graphene surface, the SWCNTs (diameters and lengths of 1.4–1.7 nm and 5–20 μm) could maximize the contact area where dislocation of the graphene surface is existed. The enhancement of the thermal conductivity due to the deposition of the SWCNTs on the graphene surface can be inferred from the previous studies.^{7,8,10,11} The previous studies revealed that the sheet resistance of the hybrid graphene/CNT was decreased compared to the graphene surface because the interconnected network of the carbon structures was formed. The decrease of the sheet resistance can be explained by the electrical conductivity enhancement. In addition, the Wiedemann–Franz law explained the relation between the electrical conductivity and the thermal conductivity. This indicates that the hybrid graphene/SWCNT heater maximized the conduction process because of its high thermal performance resulting from the interconnection of the carbon structures. Therefore, the hybrid graphene/SWCNT heater could transfer heat rapidly to the working fluid, compared with other heating surfaces.

Most studies reported that CHF enhancement was attributed to improved surface wettability,^{20–22} surface roughness,^{23,24} porous structure,^{25,26} capillary pumping limit,^{13,26,27} modulation wavelength,^{26,28} thermal properties of the heating surfaces,^{13–16,29,30} etc. To investigate the enhanced CHF and HTC of the hybrid graphene/SWCNT heating surface, the surface roughness, wettability, and thermal effusivity were considered because the other parameters (such as porous structure, capillary pumping limit, and modulation wavelength) could not be applied to the present heating surfaces. Surface roughness is a parameter that affects the active boiling center, wettability, and nucleate site density. The roughness values R_a and R_q obtained from the AFM analysis indicated that every heating surface was in the similar range. This means that the surface roughness parameter is not considered to be one of the

parameters influencing the CHF and BHT considered. Conversely, the wettability could affect the wetting and rewetting zones on the heater surface; thus, enhanced wettability could enhance the CHF performance. The static contact angle was measured to quantify the surface wettability of each heater. The contact angles (5 μL FC-72) of all heater surfaces were similar and fell in the range of 11° to 14°. Because FC-72 has a low surface tension (0.01 N/m), a liquid droplet of FC-72 spreads out over the heater surface rather than remaining as a droplet. Using FC-72 could suppress the change in surface wettability under different heater conditions. Therefore, the surface roughness and wettability are not seriously regarded as parameters that influence the CHF and HTC in the present work.

Thermal effusivity, which reflects the thermal properties of heating surfaces, was considered as the CHF and HTC enhancement parameter. The heat dissipation performance of the heater surfaces could be explained by thermal effusivity. Thermal effusivity can be defined as the rate at which a certain material can absorb and transfer heat. High thermal effusivity material delivers more heat into the coolant, and thus effective heat transfer can be observed. Effective heat dissipation on the heating surface can delay the formation of dry and hot spots, and thus enhanced heat dissipation improves the CHF and BHT. The influence of thermal conductance and capacitance can be described as the thermal effusivity^{29,30} and is given by

$$E = \sqrt{\rho_h c_h k_h} \quad (3)$$

where ρ_h , c_h and k_h are the heater material density, specific heat, and thermal conductivity, respectively. The higher effusivity heating material can increase the amount of the phase change of the fluid from liquid to vapor.^{31,32} The HTC related to the material effusivity effect was correlated in the nucleate boiling region with different working fluids.³³ This means that the HTC can be enhanced when the heating material properties are improved. For the hybrid graphene and CNTs composite, the thermal conductivity of the hybrid surface can be enhanced owing to the percolation effect triggered by the deposition of the SWCNTs on the graphene surface.¹⁵ In the present study, we combined the graphene and the SWCNTs to maximize the thermal properties of carbon structures by deposition of the SWCNTs on the graphene surface to compensate for the wrinkles and disconnected areas of the graphene surface. The main heat dissipation parameter is the thermal conductivity of the heating surface. This means that the hybrid graphene/SWCNT heating surface has the highest value of thermal effusivity because the SWCNTs connected the dislocations and wrinkles on the graphene surface. Therefore, the enhanced BHT and CHF appeared on the hybrid graphene/SWCNT heater. Thermal conductivity enhancement studies using graphene have been widely examined for the thermal management applications.^{34–36} If the enhancement methods are applied to the present heating surface, we could obtain more enhanced BHT and CHF in the hybrid graphene/SWCNT heater.

In conclusion, we demonstrated the first study of the pool boiling of a hybrid graphene/SWCNT heater, which can enhance the thermal conductivity of the surface by interconnecting the dislocation lines of the graphene. The HTC and CHF of the hybrid graphene/SWCNT heater were increased by 55% and 18%, respectively. Such enhancements can be explained by an improvement in thermal effusivity,

which influences the BHT and CHF. The hybrid graphene/SWCNT heater used in the present study will influence thermal management fields where a high power density of heating devices is needed.

AUTHOR INFORMATION

Corresponding Author

*E-mail: icbang@unist.ac.kr.

Notes

The authors declare no competing financial interest.

ACKNOWLEDGMENTS

This work was supported by the Nuclear Energy Research Program through the National Research Foundation of Korea (NRF) funded by the Ministry of Science, ICT, and Future Planning (2013M2B2B1075734, 2013M2A8A1041442, 2015M2B2A9031869).

REFERENCES

- (1) Novoselov, K. S.; Geim, A. K.; Morozov, S. V.; Jiang, D.; Zhang, Y.; Dubonos, S. V.; Grigorieva, I. V.; Firsov, A. A. *Science* **2004**, *306*, 666–669.
- (2) Geim, A. K.; Novoselov, K. S. *Nat. Mater.* **2007**, *6*, 183–191.
- (3) Balandin, A. A.; Ghosh, S.; Bao, W.; Calizo, I.; Teweldebrhan, D.; Miao, F.; Lau, C. N. *Nano Lett.* **2008**, *8*, 902–907.
- (4) Balandin, A. A. *Nat. Mater.* **2011**, *10*, 569–581.
- (5) Renteria, J. D.; Nika, D. L.; Balandin, A. A. *Appl. Sci.* **2014**, *4*, 525–547.
- (6) Kang, J.; Kim, H.; Kim, K. S.; Lee, S.; Bae, S.; Ahn, J.; Kim, Y.; Choi, J.; Hong, B. H. *Nano Lett.* **2011**, *11*, 5154–5158.
- (7) Tung, V. C.; Chen, L.; Allen, M. J.; Wasie, J. K.; Nelson, K.; Kaner, R. B.; Yang, Y. *Nano Lett.* **2009**, *9*, 1949–1955.
- (8) Kim, Y.; Min, D. *Langmuir* **2009**, *25*, 11302–11306.
- (9) Yu, D.; Dai, L. *J. Phys. Chem. Lett.* **2009**, *1*, 467–470.
- (10) Chu, K.; Li, W.; Jia, C.; Tang, F. *Appl. Phys. Lett.* **2012**, *101*, 211903.
- (11) Nguyen, D. D.; Tiwari, R. N.; Matsuoka, Y.; Hashimoto, G.; Rokuta, E.; Chen, Y.; Chueh, Y.; Yoshimura, M. *ACS Appl. Mater. Interfaces* **2014**, *6*, 9071–9077.
- (12) Chu, J. H.; Kwak, J.; Kwon, T.; Park, S.; Go, H.; Kim, S. Y.; Park, K.; Kang, S.; Kwon, S. *ACS Appl. Mater. Interfaces* **2012**, *4*, 1777–1782.
- (13) Seo, H.; Chu, J. H.; Kwon, S.; Bang, I. C. *Int. J. Heat Mass Transfer* **2015**, *82*, 490–502.
- (14) Park, S. D.; Lee, S. W.; Kang, S.; Bang, I. C.; Kim, J. H.; Shin, H. S.; Lee, D. W.; Lee, D. W. *Appl. Phys. Lett.* **2010**, *97*, 023103.
- (15) Ahn, H. S.; Jang, J.; Seol, M.; Kim, J. M.; Yun, D.; Park, C.; Kim, H.; Youn, D. H.; Kim, J. Y.; Park, G.; Park, S. C.; Kim, J. M.; Yu, D. I.; Yong, K.; Kim, M. H.; Lee, J. S. *Sci. Rep.* **2013**, *3*, 1396.
- (16) Ahn, H. S.; Kim, J. M.; Kim, J. M.; Park, S. C.; Hwang, K.; Jo, H. J.; Kim, T.; Jerng, D. W.; Kaviany, M.; Kim, M. H. *Exp. Therm. Fluid Sci.* **2015**, *60*, 361–366.
- (17) Bang, I. C.; Buongiorno, J.; Hu, L. W.; Wang, H. *JSME J. Power Energy Sys.* **2008**, *2*, 340–351.
- (18) Zuber, N. Ph.D. Thesis, Univ. of California, 1959.
- (19) Rohsenow, W. M. *Trans. ASME* **1952**, *74*, 969–976.
- (20) Kandlikar, S. G. *J. Heat Transfer* **2001**, *123*, 1071–1079.
- (21) Kim, S. J.; Bang, I. C.; Buongiorno, J.; Hu, L. W. *Int. J. Heat Mass Transfer* **2007**, *50*, 4105–4116.
- (22) Lee, C. Y.; Zhang, B. J.; Kim, J.; Kwang, J. *Exp. Therm. Fluid Sci.* **2014**, *59*, 15–23.
- (23) Chu, K.; Enright, R.; Wang, E. N. *Appl. Phys. Lett.* **2012**, *100*, 241603.
- (24) Quan, X.; Dong, L.; Chen, P. *Int. J. Heat Mass Transfer* **2014**, *76*, 452–458.
- (25) Polezhaev, Y. V.; Kovalev, S. A. *Therm. Eng.* **1990**, *37*, 617–620.
- (26) Liter, C. S.; Kaviany, M. T. *Int. J. Heat Mass Transfer* **2001**, *44*, 4287–4311.
- (27) Chen, R.; Lu, M.; Srinivasan, V.; Wang, Z.; Cho, H. H.; Majumdar, A. *Nano Lett.* **2009**, *9*, 548–553.
- (28) Park, S. D.; Bang, I. C. *Int. J. Heat Mass Transfer* **2014**, *70*, 844–850.
- (29) Golobic, I.; Bergles, A. E. *Exp. Therm. Fluid Sci.* **1997**, *15*, 43–51.
- (30) Saylor, J. R. M.S Thesis, Univ. of Minnesota, 1989.
- (31) Cossali, G. E.; Marengo, M.; Santini, M. In: *Proceedings of ILASS-Europe'05*, Orelean, France, 2005.
- (32) Cossali, G. E.; Marengo, M.; Santini, M.; Fest, S. In: *Proceedings of ICCLASS-2006*, Kyoto, Japan, 2006.
- (33) Bombardieri, C.; Manfletti, C. *Int. J. Heat Mass Transfer* **2016**, *94*, 1–8.
- (34) Goli, P.; Legedza, S.; Dhar, A.; Salgado, R.; Renteria; Balandin, A. *A. J. Power Sources* **2014**, *248*, 37–43.
- (35) Malekpour, H.; Chang, K.-H.; Chen, J. – C.; Lu, C. – Y.; Nika, D. L.; Novoselov, K. S.; Balandin, A. A. *Nano Lett.* **2014**, *14*, 5155–5161.
- (36) Renteria, J. D.; Ramirez, S.; Malekpour, H.; Alonso, B.; Centeno, A.; Zurutuza, A.; Cocemasov, A. I.; Nika, D. L.; Balandin, A. *Adv. Funct. Mater.* **2015**, *25*, 4664–4672.